Published in final edited form as:

*J Biomed Mater Res B Appl Biomater*. 2019 April ; 107(3): 818–824. doi:10.1002/jbm.b.34178.

# Cellular Response to 3-D Printed Bioactive Silicate and Borosilicate Glass Scaffolds

**Weitao Jia**[1], **Grace Y Lau**[2], **Wenhai Huang**[3], **Changqing Zhang**[1], **Antoni P Tomsia**[2], and **Qiang Fu**[2,4]

[1]Department of Orthopedic Surgery, Shanghai Jiaotong University Affiliated Sixth People's Hospital, Shanghai 200233, China

[2]Materials Sciences Division, Lawrence Berkeley National Laboratory, Berkeley, CA 94720, USA

[3]School of Materials Science and Engineering, Institute of Bioengineering and Information Technology Materials, Tongji University, Shanghai 200092, China

[4]Corning Incorporated, Corning, NY 14830, USA

## Abstract

The repair and regeneration of loaded segmental bone defects is a challenge for both materials and biomedical science communities. Our recent work demonstrated the capability of bioactive glass in supporting bone healing and defect bridging using a rabbit femur segmental defect model without growth factors or bone marrow stromal cells (BMSCs). Here in the current work, a comprehensive in vitro evaluation of bioactive silicate (13–93) and borosilicate (2B6Sr) glass scaffolds was conducted to provide further understanding of their biological performances and to establish a correlation between in vitro and in vivo behaviors. In vitro evaluation using a murine MC3T3-E1 cell line confirmed the capability of both scaffolds to support cell attachment, VEGF formation, stimulate mineral deposition and osteoblast marker gene expression. In particular, borosilicate (2B6Sr) glass showed a better capability in supporting the mineralization and gene expression than silicate (13–93) glass, consistent with a faster bone healing ability in vivo. The current in vitro results, combined with our previous in vivo findings, provide a strong basis for the further translational evaluation of bioactive glass scaffolds and for potential preclinical practice.

### Keywords

Bioactive glass; angiogenesis; mineralization

## 1. Introduction

There has been increasing interest in using bioactive glasses for the repair of both hard and soft tissues due to their unique combination of excellent bioactivity, controllable degradation and ease in forming into desired shapes[1–3]. Most of literature work, however, focuses on the use of bioactive glass in contained non-loaded sites due to the lack of sufficient

Corresponding authors: WH (whhuang@ tongji.edu.cn); CZ, (zhang_changqing@hotmail.com); QF (fuq2@corning.com).

mechanical strength[4]. Considerable efforts have been devoted to the development of porous scaffolds as bone replacement materials for tissue engineering applications [4–6]. Recent reports on the fabrication of highly strong and porous glass scaffolds using rapid prototyping technique such as direct ink writing have paved the way for their use in loaded sites[7–9]. Bioactive glass scaffolds based on 13–93 and 6P53B compositions have demonstrated mechanical strength comparable to human cortical bone while having interconnected channels composed of rectangular pores with a width of 200 μm [7, 10]. This new type of scaffold is a promising candidate for the regeneration of segmental bone defects.

Our recent in vivo work using silicate and borosilicate glass scaffolds reveals that bioactive glass scaffolds can serve as a robust bridge to heal segmental bone defect in a rabbit femur model [11]. Both glass scaffolds demonstrate a similar performance as autologous bone graft (ABG) in supporting new bone and blood vessel formation. It's interesting to note that borosilicate glass scaffolds showed a much better capability in promoting angiogenesis than silicate glass or even ABG at three months post implantation [11], suggesting their different biological performances at an early stage. In vitro study, on the other hand, serves as a fast, effective means to evaluate the performances of bioactive materials including bioactive glasses [12–14].

The present work focuses on a comprehensive in vitro evaluation of bioactive borosilicate 2B6Sr and silicate 13–93 glass scaffolds at an early stage (up to 21 days) using a murine MC3T3-E1 cell line. It is expected that the in vitro findings will shine new light on the in vivo outcomes from the same group of materials.

## 2. Materials and methods

### 2.1. Preparations and characteristics of glass scaffolds

**2.1.1 Direct-write assembly of glass scaffolds—**Bioactive 2B6Sr (composition in wt%: 15.5 $SiO_2$, 5.4 $Na_2O$, 10.8 $K_2O$, 1.2 MgO, 17.8 CaO, 4.1 $P_2O_5$, 36.2 $B_2O_3$, 9.0 SrO) and 13–93 glasses (composition in wt%: 53.0 $SiO_2$, 6.0 $Na_2O$, 12.0 $K_2O$, 5.0 MgO, 20.0 CaO, 4.0 $P_2O_5$) were purchased from SEM-COM Co. (Toledo, OH). A direct ink writing technique was used to produce scaffolds of desired dimensions, as described in details elsewhere [9]. Briefly, the inks were prepared by mixing glass particles of a $D_{50}$ = 1.2μm in a Pluronic® F-127 solution (20 wt% F-127 in di-water) at 0°C. For both glass inks, a 40 vol % solids loading was used to achieve a comparable green body density after printing. A robotic deposition device (RoboCAD 3.0, 3-D Inks, Stillwater, OK) was used to extrude the inks through a 250 μm nozzle (EFD precision tips, EFD, East Providence, RI) to produce periodic scaffolds with a spacing of 250 μm between nearest filament. After extrusion, the scaffolds were dried in air for 24 hours and then heated at 1 °C/min to 600 °C to decompose the organic polymers before sintering at 620 °C for 2 hour (2B6Sr glass) or 700 °C for 1 hour (13–93 glass).

Square plates (6 mm × 6 mm × 2 mm) of scaffolds samples were prepared for cell culture by sectioning and surface grinding the sintered scaffolds. All of the scaffolds were washed 3 times with deionized water and ethanol, and were dry-heat sterilized prior to experiments.

**2.1.2. Microstructural measurements—**Scanning electron microscopy, SEM (Hitachi S-4300, Tokyo, Japan), was used to observe the microstructure of the scaffolds. Archimedes method was used to measure the porosity of the sintered glass scaffolds. Additionally, 3-D perspective of the scaffolds was obtained using synchrotron X-ray micro-computed tomography (SR micro-CT), which was conducted at the Advanced Light Source (ALS-LBNL, Berkeley, CA) with 22 keV monochromatic X-rays and a 4.4 μm voxel size (resolution). The images were reconstructed using Octopus and the 3-D structural view was realized using Avizo™.

**2.1.3. Mechanical properties testing—**Cubical blocks (3 mm × 3 mm × 3 mm) were measured for compressive strength at room temperature using a servo-hydraulic testing machine (MTS810, MTS Systems, Eden Prairie, MN) at a cross-head speed of 0.5 mm/min with a load cell of 500 lb. At least 20 samples were tested to evaluate their mechanical reliability using a Weibull distribution.

The Weibull modulus in each type of scaffolds was determined according to ASTM C1239–07 by fitting the strength data with the equation [15]:

$$\ln\ln\left(\frac{1}{1-P_f}\right) = m\ln\left(\frac{\sigma}{\sigma_0}\right)$$

where $P_f$ is the probability of failure at a stress $\sigma$, $\sigma_0$ the Weibull scale parameter determined from the intercept of the fit to the data and $m$ the Weibull modulus. The value $\sigma_0$ is also the stress at which the probability of failure is 63%. $P_f$ was evaluated using the equation:

$$P_f = \frac{i-0.5}{n}$$

where $n$ is the total number of specimens and $i$ the specimen rank in ascending order of failure stress.

## 2.2. In vitro evaluation of cell growth and function on glass scaffolds

**2.2.1. Cell culture and attachment assay—**The established MC3T3-E1 line of murine pre-osteoblastic cells was obtained from ATCC and cultured in α-MEM medium supplemented with 10% fetal bovine serum, 100 U/ml penicillin and 100 μg/ml streptomycin sulfate (Gibco, BRL, USA) in a humidified 5% $CO_2$ balanced-air incubator at 37 ºC, with the medium being changed every other day. The scaffolds were seeded with $1.0\times10^5$ MC3T3-E1 cells suspended in 100 μl of complete medium, and incubated for 4 h to permit cell attachment. The cell seeded scaffolds were then transferred to a 24-well plate containing 2 ml of complete medium per well. The control group consisted of the same number of cells seeded in wells containing 2 ml of α-MEM medium. At culture intervals of 3, 7 and 14 days, glass scaffolds with attached cells were removed, rinsed twice with warm phosphate-buffered saline (PBS), and soaked overnight in 2.5% glutaraldehyde in PBS. The fixed samples were then rinsed with PBS three times and dehydrated with a graded tetra butyl alcohol series. The samples were allowed to dry in air for 12 h at room temperature, sputter-

coated with Au/Pd, and then observed using SEM (Quanta 200 FEG, FEI Co., The Netherlands) at 5 kV accelerating voltage.

**2.2.2. MTT assay—**To evaluate the metabolically active MC3T3-E1 cells on and within the porous scaffolds, a MTT assay was conducted to determine cell proliferation. At designated time of 1, 3 and 7 days, the cell-seeded scaffolds and control wells were placed in 400 μl serum-free medium containing 100 μg of the tetrazolium salt MTT (Sigma, USA; 5mg/ml) for the last 4 h of incubation to permit visualization of metabolically active cells. After the incubation, the scaffolds were briefly rinsed in warm PBS and blotted dry. The insoluble purple formazan, a product of mitochondrial MTT metabolism, was extracted from the scaffolds with 1.0 ml ethanol and measured spectrophotometrically for optical density (OD) values at 490 nm in microplate reader (Bio-Tek, USA).

**2.2.3. Measurement of VEGF production and ALP activity—**In vitro protein levels of VEGF secreted by MC3T3-E1 cells seeded on glass scaffolds during a 24-h period was quantified in conditioned medium at 1, 3, 7 and 14 days using ELISA kit (antibodiesonline, Aachen, Germany), according to the manufacturer's instructions. Cells cultured on culture plate without glass scaffolds were used as control.

ALP activity was measured to assess the effects of glass scaffolds on osteogenesis capacity of MC3T3-E1. After osteogenic induction culture (Gibco BRL, USA), cell-seeded scaffolds were removed at 7 and 14 days and rinsed twice with warm PBS. Cells were lysed twice using freeze-thaw cycle at −80/37ºC with 500 μl of 1 % Triton X-100 in PBS. The total amount of protein in lysates recovered from the cell-seeded scaffolds was measured using a Micro BCA Protein Assay Kit (Thermo Fisher, USA), following the manufacturer's instructions. ALP activity was determined at 405 nm in microplate reader (Bio-Tek, USA) using 0.5 M 2-amino-2-methyl-l-propanol (AMP) buffer containing 50 mM p-nitrophenyl phosphate (p-NPP) (Sigma-Aldrich, USA) as the substrate. The ALP values were normalized against protein concentration.

**2.2.4. Mineralized bone-like tissue observation—**To assess the ability of the glass scaffolds to support mineralization of MC3T3-E1 cells, the cell-seeded scaffolds were cultured in osteogenic induction medium. The medium was changed every 2 days. After incubating for 14 and 21 days, the medium was replaced by tetracycline solution (50 μg/ml) and incubated for 30 min, followed by washing with PBS, and the cells were fixed in 95% ethanol. The mineral deposition was observed using a fluorescent microscope (Leica DMI 6000B, Germany). The area of the mineral deposition was calculated using the image analysis software (Image-Pro Plus, Germany) and was expressed as the percentage of each measurable area in a randomly selected field.

**2.2.5. RNA isolation and real-time PCR analyses—**To further analyze the differentiation of MC3T3-E1 cells on the scaffolds, RT-PCR was used to assess mRNA expression of osteogenic gene markers. After incubating 7, 14 and 21 days in osteogenic induction medium, the cell-seeded scaffolds and control cells were washed twice with warm PBS. Total cellular RNA was extracted using RNAiso Plus (Takara Bio, Japan), following the instructions provided. Complementary DNA was synthesized using PrimeScrip RT

Reagent Kit (Takara Bio, Japan) on a PTC-200 Peltier Thermal Cycler PCR machine (Bio-Rad, USA). RT-PCR was then performed using a quantitative real-time amplification system (LightCycler 480, Switzerland) with SYBR-Green Premix Ex Taq II (Takara Bio, Japan). The conditions for RT-PCR were 40 cycles at 95 ºC for 10 s, 60 ºC for 20 s and 72 ºC for 20s. GAPDH was used as the internal control. The primers sequences for RT-PCR were synthesized commercially (Shengong, Co. Ltd. Shanghai, China) as follows:

1) GAPDH fwd 5' ATGGGGAAGGTGAAGGTCG 3', GAPDH rev 5' GGGGTCATTGATGGCAACAATA 3', 2) Core binding factor I (CBFA1) fwd 5′CGCATTCCTCATCCCAGTAT3′, CBFA1 rev 5'GGTGGCAGTGTCATCATCTG3', 3) Bone sialoprotein (BSP) fwd 5'GAGCCAGGACTGCCGAAAGGAA 3', BSP rev 5'CCGTTGTCTCCTCCGCTGCTGC3', 4) Alkaline phosphatase (ALP) fwd 5'GCCCTCTCCAAGACATATA3', ALP rev 5'CCATGATCACGTCGATATCC3', 5) Collagen type I (COL I) fwd 5'GAGGCATAAAGGGTCATCGTGG 3', COL I rev 5' CATTAGGCGCAGGAAGGTCAG3', 6) Osteocalcin (OCN) fwd 5'CAGCTTGGTGCACACCTAGC3', OCN rev 5'AGGGTTAAGCTCACACTGCTCC3'.

PCR products were then electrophoresed on a 1.2% agarose gel and visualized by ethidium bromide fluorostaining. The density of bands was determined using densitometry and Gel-Pro analyzer software.

### 2.4. Statistical analysis

Statistical analysis was performed using Statistical Package for the Social Sciences, Version 11.0 for Windows (SigmaStat, SPSS Science, Chicago, IL). Data were collected from at least triplicate parallel samples in vitro or six samples in vivo. The results were reported as the mean ± standard deviation (SD). Values were considered to be significant when $p < 0.05$.

## 3. Results

### 3.1. Bioactive glass scaffolds

Figure 1 shows the structure of 13–93 glass scaffold fabricated using a direct-ink-writing technique. Micro-CT and SEM images demonstrate the presence of a well-defined hierarchical structure in the scaffold. The 2B6Sr glass scaffold (not shown here) has a similar microstructure as 13–93 in order to eliminate the structural impact on their biological performances. Both scaffolds have an open porosity > 50 with large square pores (200 μm) and small rectangular pores (40 – 60 μm × 150 μm. The compressive strength and the elastic modulus measured parallel to the pore channels were 80.4 MPa and 4.7 GPa for 13–93 glass scaffolds, 35.6 MPa and 1.6 GPa for 2B6Sr glass scaffolds, respectively. Glass scaffolds used in this study had strength values at least five to 10 times those of HA or β-TCP ceramic constructs reported in literature [9].

The distribution of compressive strength values of both 13–93 and 2B6Sr glass scaffolds exhibited a low scatter (Figure 2). Weibull modulus ($m$) of 6.0 and 4.3 for 13–93 and 2B6Sr scaffolds, respectively, were determined from the plot of $ln[-ln(1-p)]$ versus $ln\sigma$.

### 3.2. In vitro evaluation

**3.2.1. Cell morphology—**Both types of glass scaffolds demonstrated excellent capability in supporting the growth and attachment of the MC3T3, a murine pre-osteoblastic cell line. Cellular attachment and interaction within glass scaffolds were observed by SEM (Figure 3). Small clusters of cells could be seen attaching to the surface of both glass scaffolds at low density after culturing for three days, indicative of favorable cytocompatibility (Figure 3 a1, b1). Numerous cell projections along the walls of the scaffolds were observed, suggesting firm cell attachment to the scaffolds. The morphology of cells grown on 2B6Sr glass scaffolds was generally similar to that on 13–93 glass scaffolds. The cells density increased with incubation time and, after seven days, the cells grew along and covered the pore walls of the scaffolds, reaching confluence with abundant fibril networks of extracellular matrix deposited on the scaffolds and contacting with adjacent cells (Figure 3 a2, b2). The surface and the interior of the scaffolds were almost completely covered with cells, aggregating with other cells via multiple extensions of pseudopodia after 14 days (Figure 3 a3, b3).

**3.2.2. Cell proliferation and differentiation on glass scaffolds—**Quantitative evaluation of the two glass scaffolds to support cell proliferation, differentiation, mineralization and angiogenesis was conducted using MTT, ALP, tetracycline fluorescence labeling and VEGF assays, respectively. MTT assay demonstrates a linear increase in the OD values with incubation time (Figure 4a). The OD values from both scaffolds were significantly higher than those of cells control after 3 days ($p<0.05$), evidence of an increasing number of cells grown in both glass scaffolds. A higher OD value was also observed from 2B6Sr scaffold than from 13–93 scaffold after 7 days of culture ($p<0.05$), indicating a better capability of the former in supporting cell proliferation (Figure 4a).

ALP activity of MC3T3-E1 cells seeded on the two glass scaffolds increased significantly with incubation time (Figure 4b), suggesting their ability to promote cell differentiation. ALP levels measured from both scaffolds were significantly higher than those of control cells without scaffolds at both time points. Higher ALP levels were also observed from 2B6Sr scaffolds than that of 13–93 scaffolds at day 14 ($p<0.05$) (Figure 4b).

Consistent with the findings from ALP assay, significant increase in the area percentage of mineral deposition on the surface of the scaffolds was observed after osteogenic induction culture from day 14 to 21 (Figure 4c). The values measured from both scaffolds were significantly higher than those of control cells at both time points, and the value was also significantly higher for 2B6Sr scaffolds compared with 13–93 scaffolds at 21 days ($p<0.05$) (Figure 4c and 5a-c).

The ability of the two scaffolds to promote angiogenesis was assessed using a VEGF assay, as shown in Figure 4d. VEGF production in conditioned medium increased significantly in both scaffolds groups till 7 days and the values of glass scaffolds were significantly higher than that of control cells after 7 days ($p<0.05$). At 14 days, the VEGF value of 2B6Sr scaffolds was also significantly higher than that of 13–93 scaffolds group ($p<0.05$) (Figure 4d).

**3.2.3. RNA isolation and Real-time PCR analyses—**The results of RT-PCR analyses for osteogenic gene markers (Figure 6) showed that the expression levels of key osteogenic transcripts for CBFA I, ALP and OCN increased in cells seeded on both glass scaffolds from 7 to 21 days. Especially for ALP and OCN, it showed sustained marked upregulation in cells seeded on 2B6Sr glass scaffolds, but moderate upregulation in 13–93 glass scaffolds. The mRNA for all osteogenic gene markers at all time intervals, with the exception of CBFA I and ALP at 7 days, were higher in 2B6Sr group than 13–93 group, and both scaffolds groups were higher than those of control cells. The transcripts of BSP and COL I showed an initial high expression at 7 days especially in 2B6Sr glass scaffolds, and thereafter downregulation till 21 days in all groups.

## 4. Discussion

This study investigated the cellular response to two types of glass scaffolds with comparable structure but of different glass compositions. In vitro cell culture using MC3T3 cells confirmed the ability of both 13–93 and 2B6Sr glass scaffolds in promoting cell attachment, proliferation, differentiation and mineralization (Figure 3–6). This is in general agreement with previous studies [12, 13], indicating the excellent bioactivity of both glasses. The present work also revealed that a Sr-containing borosilicate 2B6Sr glass performed similar to or better than silicate 13–93 glass, which is different from the literature reports that borate or borosilicate glass showed less capability in supporting in vitro cell culture than silicate glass using an MC3T3-E1 or osteogenic MLO-5 cell line [16, 17]. Significantly higher values of MTT, ALP and mineralized area were observed from 2B6Sr than from 13–93 scaffolds at designated time points, suggesting the released strontium could result in improved proliferation and mineralization of MC3T3-E1 cells. This was further supported by the higher expression levels of key osteogenic gene markers detected from RT-PCR analyses.

As the two types of glass scaffolds exhibit a comparable microstructure and porosity, their different in vitro performances are likely due to the different glass chemistry. The release of soluble Si, Ca, P, and Na ions as a result of glass surface reaction and degradation is reported to give rise to the osteoinductive and osteogenic properties in bioactive glass[1, 2, 18]. The 2B6Sr composition is substations of two-thirds of $SiO_2$ with $B_2O_3$ and three quarters of MgO with SrO in 13–93 composition while keeping the rest oxides the same. As a trace element in the human body, Sr is reported to accumulate in bone and replace calcium in metabolic process[19], and to stimulate cell proliferation and differentiation[20–24]. Both $B_2O_3$ and SrO have been reported to stimulate bone ingrowth in recent studies [20–26]. The addition of $B_2O_3$ was also reported to increase glass degradation rate as confirmed by previous studies[27, 28]. A combination of fast ion release and the presence of Sr ions are believed to account for a better in vitro performance in 2B6Sr than in 13–93 glass scaffolds, which implies its better capability in supporting in vivo bone regeneration. This echoes their in vivo behaviors with more blood vessels formed in 2B6Sr at an early stage [11], strong evidence that glass compositions have a drastic impact on their in vitro and in vivo functions.

## 5. Conclusions

Silicate 13–93 and borosilicate 2B6Sr glass scaffolds with precisely controlled 3-D architecture and outstanding mechanical strength were produced using a direct-ink-writing technique. Both glass scaffolds demonstrate excellent capability in supporting the MC3T3-E1 cells proliferation, mineral deposition and high expression of key osteogenic gene markers in vitro. It's worth noting that borosilicate glass demonstrated better in vitro performance than silicate glass for the period of study (up to 21 days). The encouraging results from this work pave the way to the further evaluation of bioactive glass scaffolds for the reconstruction of large bone defects in both large animal models and pre-clinical practice.

## Acknowledgement:

This work was supported by the National Institutes of Health/National Institute of Dental and Craniofacial Research (NIH/NIDCR) Grant No. 1R01DE015633, and the Natural Science Foundation of China Grant No. 81572105, 51072133, 81000811 and 51372170, and Shanghai Municipal Education Commission - Gaofeng Clinical Medicine Grant Support (Grant No. 20172026) and Shanghai Talents Development Fund (Grant No. 2017035).

## References:

1. Rahaman MN, et al., Bioactive glass in tissue engineering. Acta Biomater, 2011 7(6): p. 2355–73. [PubMed: 21421084]
2. Jones JR, Review of bioactive glass: From Hench to hybrids. Acta Biomaterialia, 2013 9(1): p. 4457–4486. [PubMed: 22922331]
3. Miguez-Pacheco V, Hench LL, and Boccaccini AR, Bioactive glasses beyond bone and teeth: emerging applications in contact with soft tissues. Acta Biomaterialia, 2015 13: p. 1–15. [PubMed: 25462853]
4. Fu Q, et al., Toward Strong and Tough Glass and Ceramic Scaffolds for Bone Repair. Advanced Functional Materials, 2013 23(44): p. 5461–5467. [PubMed: 29527148]
5. Fu Q, et al., Bioactive glass scaffolds for bone tissue engineering: state of the art and future perspectives. Mater Sci Eng C Mater Biol Appl, 2011 31(7): p. 1245–1256. [PubMed: 21912447]
6. Hutmacher DW, Scaffolds in tissue engineering bone and cartilage. Biomaterials, 2000 21(24): p. 2529–2543. [PubMed: 11071603]
7. Fu Q, Saiz E, and Tomsia AP, Bio-inspired Highly Porous and Strong Glass Scaffolds. Adv Funct Mater, 2011 21: p. 1058–1063. [PubMed: 21544222]
8. Deliormanli AM and Rahaman MN, Direct-write assembly of silicate and borate bioactive glass scaffolds for bone repair. Journal of the European Ceramic Society, 2012 32(14): p. 3637–3646.
9. Fu Q, Saiz E, and Tomsia AP, Direct ink writing of highly porous and strong glass scaffolds for load-bearing bone defects repair and regeneration. Acta Biomaterialia, 2011 7(10): p. 3547–3554. [PubMed: 21745606]
10. Liu X, et al., Mechanical properties of bioactive glass (13–93) scaffolds fabricated by robotic deposition for structural bone repair. Acta Biomaterialia, 2013 9(6): p. 7025–7034. [PubMed: 23438862]
11. Jia W, et al., Bioactive Glass for Large Bone Repair. Advanced Healthcare Materials, 2015 4(18): p. 2842–2848. [PubMed: 26582584]
12. Fu HL, et al., In vitro evaluation of borate-based bioactive glass scaffolds prepared by a polymer foam replication method. Materials Science & Engineering C-Materials for Biological Applications, 2009 29(7): p. 2275–2281.
13. Fu Q, et al., Silicate, borosilicate, and borate bioactive glass scaffolds with controllable degradation rate for bone tissue engineering applications. I. Preparation and in vitro degradation. Journal of Biomedical Materials Research Part A, 2010 95A(1): p. 164–171.

14. Chen QZZ, Thompson ID, and Boccaccini AR, 45S5 Bioglass (R)-derived glass-ceramic scaffolds for bone tissue engineering. Biomaterials, 2006 27(11): p. 2414–2425. [PubMed: 16336997]
15. International, A., *Standard practice for reporting uniaxial strength data and estimating Weibull distribution parameters for advanced ceramics*, 2007.
16. Brown RF, et al., Effect of borate glass composition on its conversion to hydroxyapatite and on the proliferation of MC3T3-E1 cells. Journal of Biomedical Materials Research Part A, 2009 88(2): p. 392–400. [PubMed: 18306284]
17. Fu QA, et al., Silicate, borosilicate, and borate bioactive glass scaffolds with controllable degradation rate for bone tissue engineering applications. II. In vitro and in vivo biological evaluation. Journal of Biomedical Materials Research Part A, 2010 95A(1): p. 172–179.
18. Hench LL and Polak JM, Third-generation biomedical materials. Science, 2002 295(5557): p. 1014–1017. [PubMed: 11834817]
19. Lao J, Jallot E, and Nedelec J-M, Strontium-Delivering Glasses with Enhanced Bioactivity: A New Biomaterial for Antiosteoporotic Applications? Chemistry of Materials, 2008 20(15): p. 4969–4973.
20. Gentleman E, et al., The effects of strontium-substituted bioactive glasses on osteoblasts and osteoclasts in vitro. Biomaterials, 2010 31(14): p. 3949–3956. [PubMed: 20170952]
21. Newman SD, et al., Enhanced osseous implant fixation with strontium-substituted bioactive glass coating. Tissue Engineering - Part A, 2014 20(13–14): p. 1850–1857. [PubMed: 24471799]
22. Autefage H, et al., Sparse feature selection methods identify unexpected global cellular response to strontium-containing materials. Proceedings of the National Academy of Sciences, 2015 112(14): p. 4280–4285.
23. Naruphontjirakul P, Porter AE, and Jones JR, *In* vitro osteogenesis by intracellular uptake of strontium containing bioactive glass nanoparticles. Acta Biomaterialia, 2018 66: p. 67–80. [PubMed: 29129790]
24. Stefanic M, et al., The influence of strontium release rate from bioactive phosphate glasses on osteogenic differentiation of human mesenchymal stem cells. Journal of the European Ceramic Society, 2018 38(3): p. 887–897.
25. Bi L, et al., Evaluation of bone regeneration, angiogenesis, and hydroxyapatite conversion in critical-sized rat calvarial defects implanted with bioactive glass scaffolds. Journal of Biomedical Materials Research Part A, 2012 100A(12): p. 3267–3275.
26. Bonnelye E, et al., Dual effect of strontium ranelate: stimulation of osteoblast differentiation and inhibition of osteoclast formation and resorption in vitro. Bone, 2008 42(1): p. 129–138. [PubMed: 17945546]
27. Liu X, Rahaman MN, and Day DE, Conversion of melt-derived microfibrous borate (13–93B3) and silicate (45S5) bioactive glass in a simulated body fluid. Journal of Materials Science: Materials in Medicine, 2013 24(3): p. 583–595. [PubMed: 23233025]
28. Stone-Weiss N, et al., Understanding the structural drivers governing glass–water interactions in borosilicate based model bioactive glasses. Acta Biomaterialia, 2018 65: p. 436–449. [PubMed: 29127067]

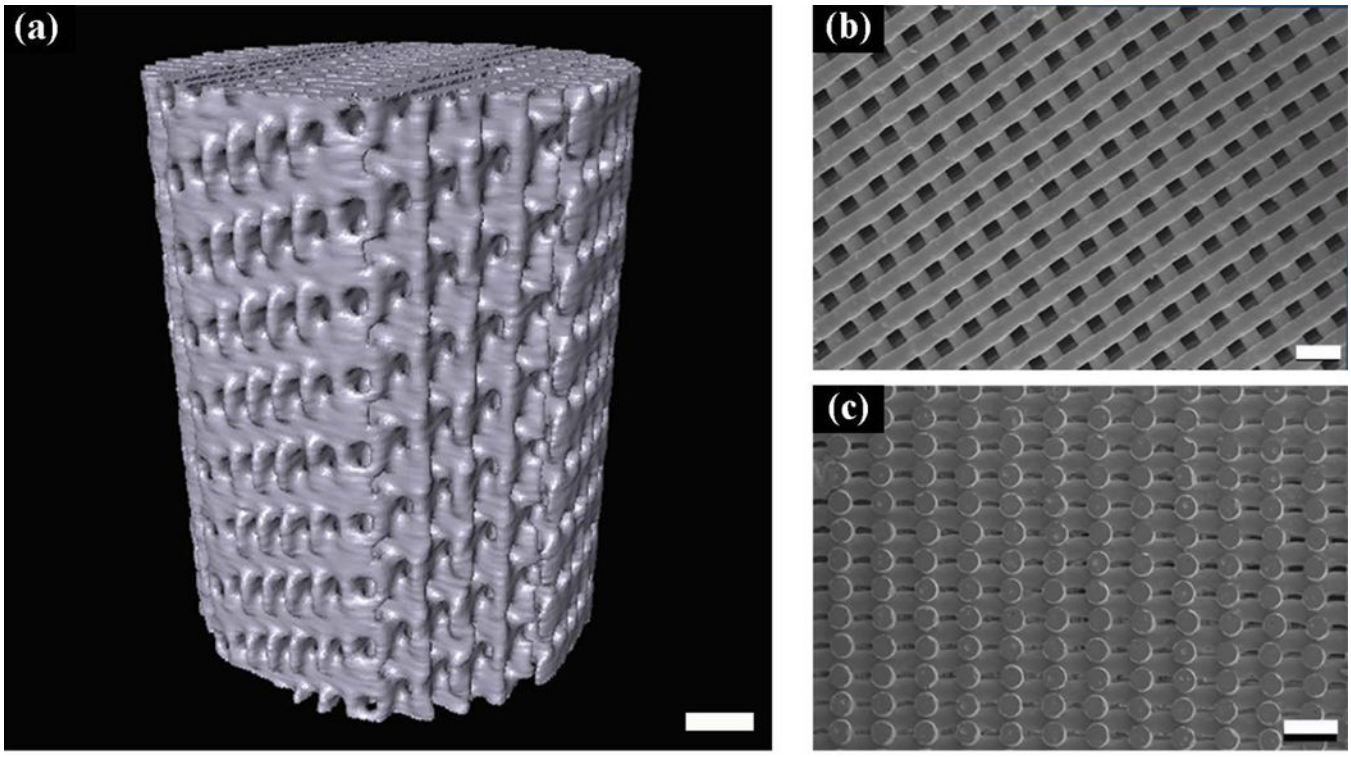


**Figure 1.**

Bioactive glass scaffolds used in the present work. (a) A 3-D view of a 13–93 glass scaffold using synchrotron X-ray tomography; SEM images showing: (b) top and (c) side views of a 13–93 glass scaffold. Scale bar: 1mm in (a); 500 um in both (b) and (c).

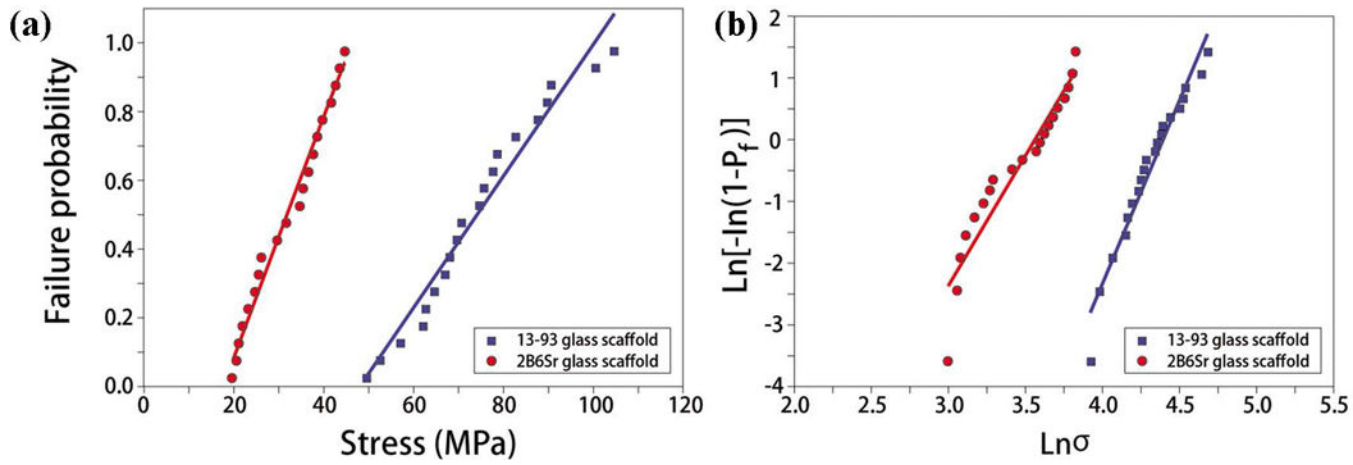


**Figure 2.**

Weibull distribution (a) and logarithmic plots for compressive strength values of 13–93 and 2B6Sr glass scaffolds (b).

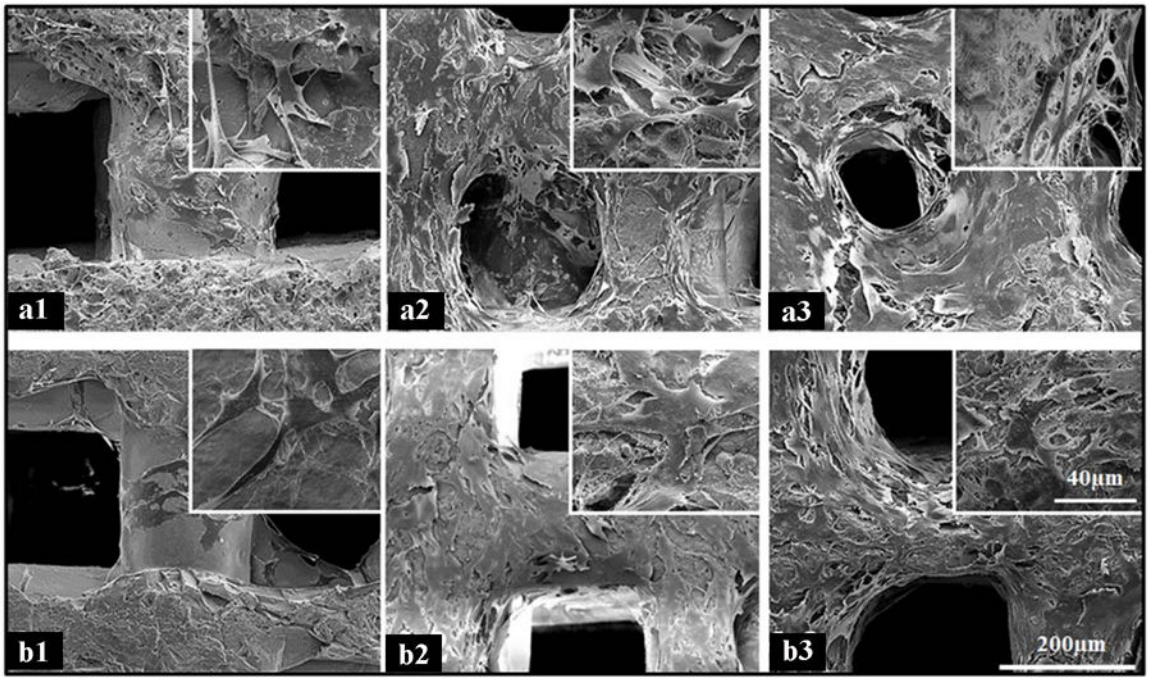


**Figure 3.**

SEM micrographs of 2B6Sr (a) and 13–93 (b) glass scaffolds after seeding with MC3T3-E1 cells for 3 days (a1 and b1), 1 week (a2 and b2) and 2 weeks (a3 and b3), showing the cells attaching and spreading along the struts and pores up to reaching confluence with adjacent cells (500×for a and b; 3000×for insets).

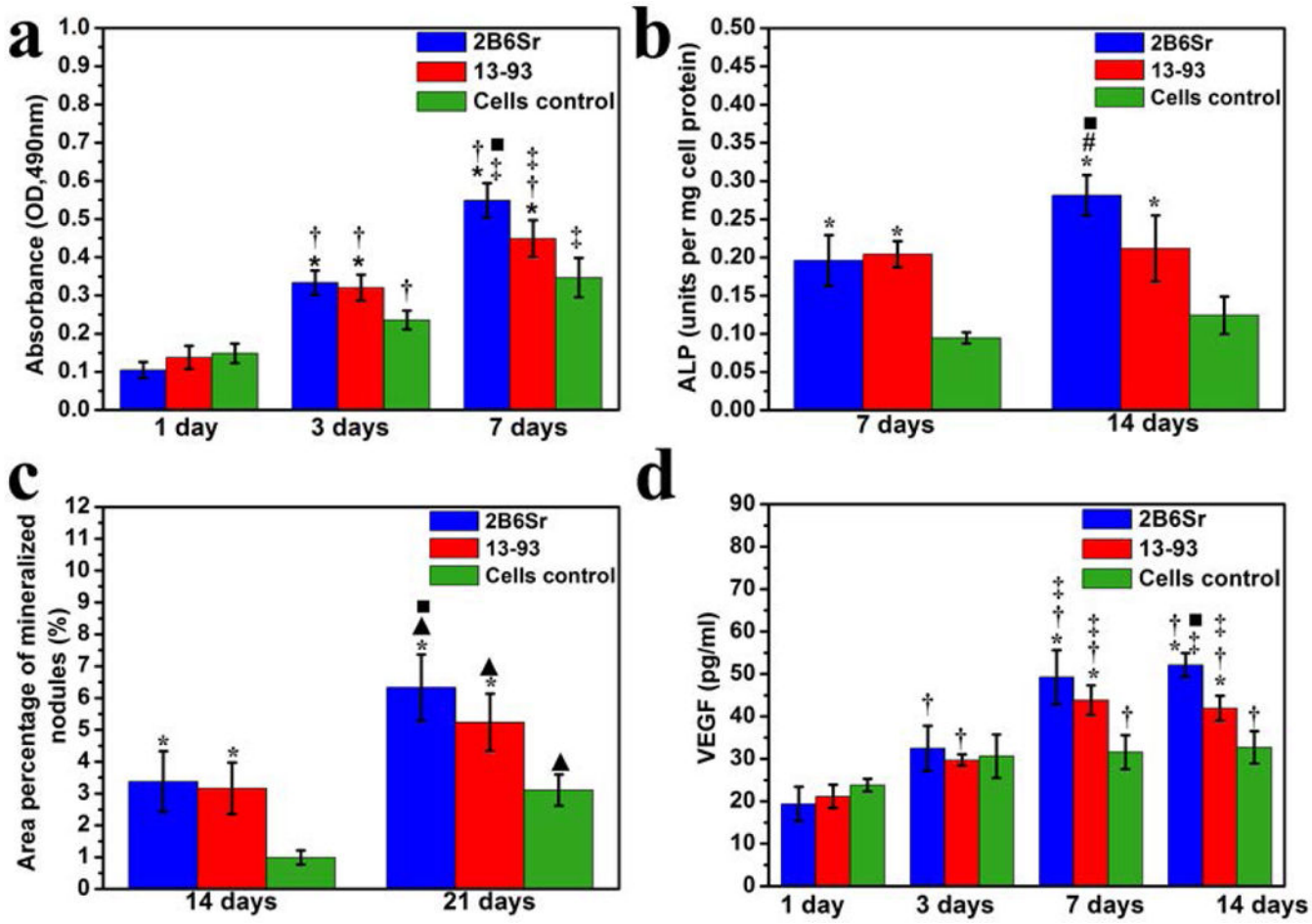


**Figure 4.**

Quantitative analysis of MC3T3-E1 cells cultured on 2B6Sr and 13–93 glass scaffolds at designate time points for proliferation by MTT assay (a) and VEGF production (b), ALP activity (c) and mineral deposition (d) after osteogenic induction culture. * indicates statistically significance compared with cells control ($p<0.05$); † indicates statistically significance compared with themselves at 1 day ($p<0.05$); ‡ indicates statistically significance compared with themselves at 3 days ($p<0.05$); # indicates statistically significance compared with themselves at 7 days ($p<0.05$); ▲ indicates statistically significance comparedwith themselves at 14 days ($p<0.05$); ■ indicates statistically significance between 13–93 and 2B6Sr group ($p<0.05$).

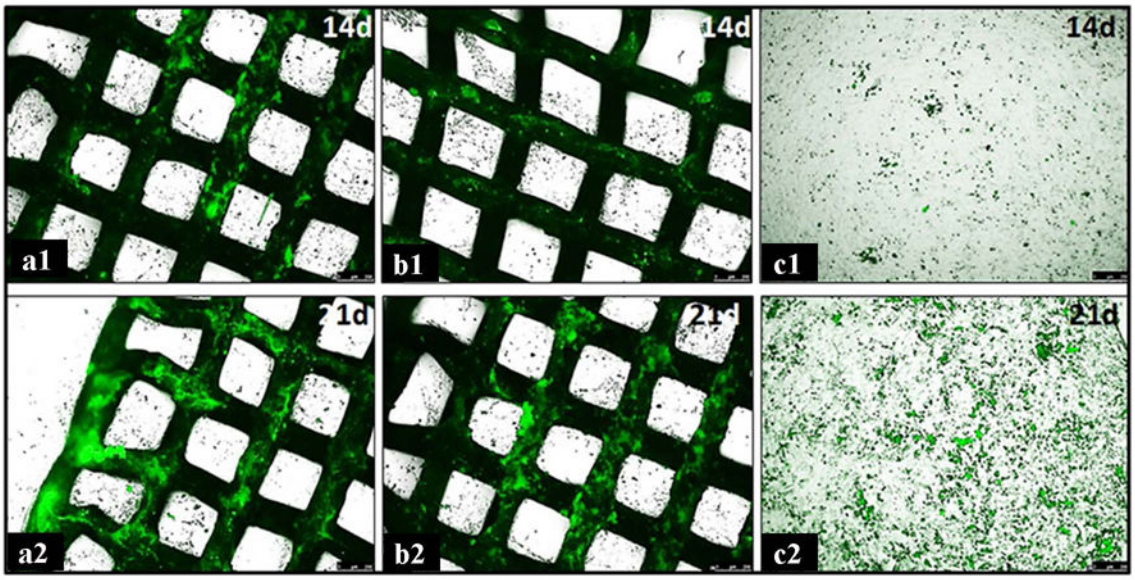


**Figure 5.**

Tetracycline fluorescence microphotographs of mineral deposition of MC3T3-E1 cells after culturing on surface of 2B6Sr (a1 and a2), 13–93 (b1 and b2) scaffolds and on bottom of culture dish (c1 and c2) at 14 and 21 days, respectively.

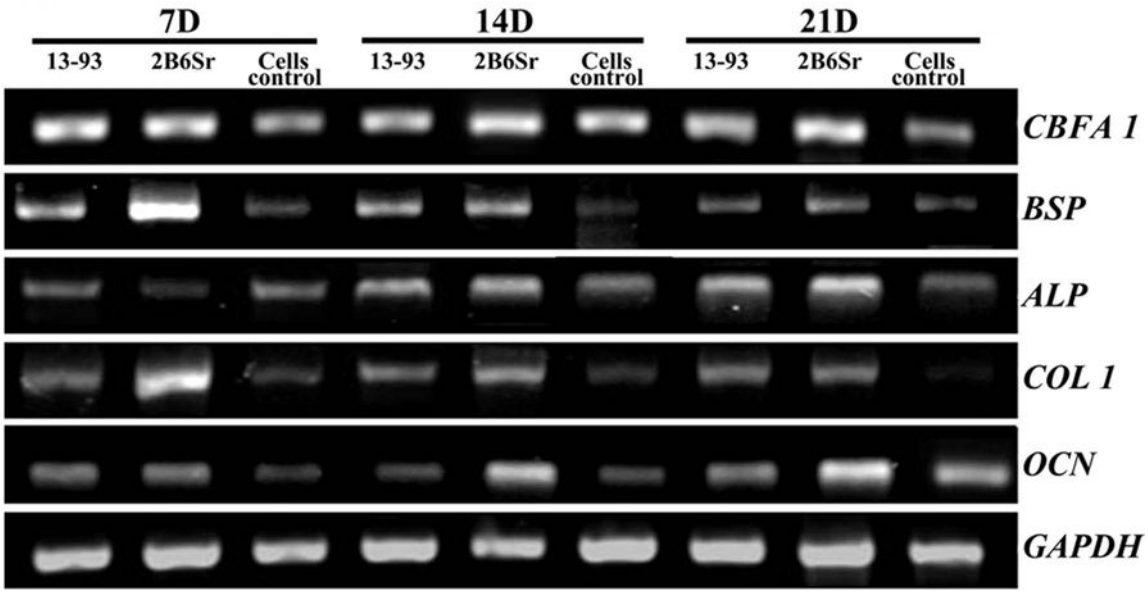


**Figure 6.**

Osteogenic marker gene expression of MC3T3-E1 cells cultured on both glass scaffolds in osteogenic induction medium for 7, 14 and 21 days, respectively.